JPE 15-6-20

http://dx.doi.org/10.6113/JPE.2015.15.6.1601
ISSN(Print): 1598-2092 / ISSN(Online): 2093-4718

PQ Control of Micro Grid Inverters with Axial Voltage Regulators

Yang Chen*, Jinbin Zhao†, Keqing Qu*, and Fen Li*

*,†Department of Electrical Engineering, Shanghai University of Electric Power, Shanghai, China

Abstract

This paper presents a PQ control strategy for micro grid inverters with axial voltage regulators. The inverter works in the voltage-controlled mode and can help improve the terminal power quality. The inverter has two axial voltage regulators. The 1st regulator involves the output voltage amplitude and output impedance, while the 2nd regulator controls the output frequency. The inverter system is equivalent to a controllable voltage source with a controllable inner output impedance. The basic PQ control for micro grid inverters is easy to accomplish. The output active and reactive powers can be decoupled well by controlling the two axial voltages. The 1st axial voltage regulator controls the reactive power, while the 2nd regulator controls the active power. The paper analyses the axial voltage regulation mechanism, and evaluates the PQ decoupling effect mathematically. The effectiveness of the proposed control strategy is validated by simulation and experimental results.

Key words: Axial voltage regulator, PQ decoupling, Single phase inverter, Voltage-controlled

I. INTRODUCTION

With the rapid development of smart grid and civil distributed generation, micro grids have become a popular trend for distribution networks [1]. A microgrid usually consists of distributed photovoltaic generators, wind turbines, combined heat and power plants, fuel batteries and so on. A microgrid is usually connected to the main grid and the main grid provides frequency and amplitude support for the microgrid. It does not have as many traditional synchronous generators as the main grid. When grid faults occur, a microgrid works in the stand-alone mode and becomes easy to collapse. Commonly used current-controlled inverters (CCI) [2]-[4] are current sources which only supply power and cannot help to provide transient support. Voltage-controlled inverters (VCI) can be regarded as voltage sources which can provide voltage support in urgent circumstances [5]-[8].

Inverter-based distributed generators are the main power suppliers of microgrids. Nowadays the inverters applied in microgrids are often paralleled without control interconnection. Thus, the *P-f* droop control, which roughly mimics output characteristic of traditional synchronous generators, is widely used. However, this does have a lot of problems in terms of power sharing and many other aspects [9]. The distributed generators for microgrids are not far away from each other. With the development of communication technology, interconnected inverters will be widely used in microgrids. Thus, inverters will often work in the PQ output mode. The PQ references are from the MPPT control or the upper scheduling centers.

The control strategies referred to as virtual synchronous generators (VSG) [10]-[12] are developed for microgrid. Most VSG inverters are voltage sources and can help to maintain the stability of microgrids. By using the VSG control strategy, the mature control strategies developed for the main grid can be applied in microgrids as well. Ref. 10 introduced the idea of the VSG mainly based on the rotor equation. Nowadays, the concept of a 'synchronverter' [11] is well known. It is a converter that mimics both the inertial equation and electromagnetic transient process of synchronous generators. However, the inner output impedance of the inverter is the real filter inductor and it is not controllable. In addition, the paper only discussed the inner output power while the filter impact on the active and reactive power output is neglected.

Reference [13] has proposed a single-phase voltage

Manuscript received Mar. 17, 2015; accepted Jun. 10, 2015
Recommended for publication by Associate Editor Yujin Song.
†Corresponding Author: zhaojinbin@shiep.edu.cn
Tel: +86-189-6485-8856, Shanghai University of Electric Power
*Dept. of Electrical Eng., Shanghai University of Electric Power, China

controlled inverter with an inner output impedance. The inverter has many great characteristics. However, further control strategies have not been researched yet. This paper improves the control strategy of Reference [13]. The hysteresis PWM is replaced by the commonly used SPWM method, and the inverter side inductor current is adopted as the feedback value of the inner current loop. The SOGI is adopted for quadrature signal generation. The working principle of the axial voltage regulators is further analyzed and a basic *PQ* control strategy for microgrids is proposed and discussed in detail.

Section II will discuss the whole inverter system and the 1st axial voltage regulator control strategy. Frequency regulation improvement and analysis will be presented in Section III. The details of the *PQ* control based on axial voltage regulators will be discussed in Section IV. Simulation and experiment results will be given in Section V. Finally, some conclusions are given in Section VI.

II. System Description and 1ST Axial Voltage Regulator Control Strategy

The main circuit and control strategy are shown in Fig. 1. Here the voltage of the DC bus is regarded as a constant. A LCL filter is used for the single phase inverter. The current through inductor L_1 is measured for the PWM generation. A small L_2 is chosen so that v_o is nearly the same as v_g. Since the inverter is designed mainly for microgrids and civil distributed generation, the nominal power rate is small. Thus, a resister cascaded with the capacitor will not cause a large power loss but will greatly help simplify the inverter design. The output voltage v_o and output current i_o are measured. The output P & Q are calculated and compared with the reference values. Then they are sent into the main control strategy through 2 PI controllers. As described in reference [8], here in Fig. 1, V_1^* and V_2^* are the input values of the axial voltage regulators. V_1^* controls the amplitude of the equivalent voltage, while V_2^* regulates the output frequency. The whole control strategy of the V_1^* regulator is shown in Fig. 2 while details of the V_2^* regulator will be discussed in the next section.

The detailed control strategy of the V_1^* regulator is shown in Fig. 2. Here in Fig 2, V_1^* and E_N have been multiplied by the phase information from the V_2^* regulator, which will be discussed in the next section. The reference of V_1^* came from the output power loop. K_{mu1} is the V_1^* regulation coefficient. It can help regulate the effect of the output voltage v_o more flexibly. α is the PI gain, and *Ti* is the integral time constant. These two are the main parameters for the inner impedance design. β and γ are the feedback coefficients of the output current and the filter capacitor current. They will help simplify the output expression.

V_1^* contains information from the outer power loop. It is

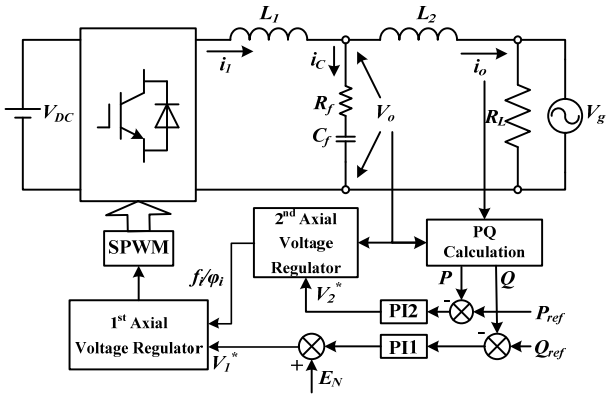

Fig. 1. The system and the whole control strategy.

multiplied with the output voltage v_o to form a voltage reference signal, and the voltage reference signal is sent to the PI controller after adding the nominal voltage. The output of the PI controller with feedback from the capacitor current and output current forms the reference current of the inner current loop.

By this control strategy, equation (1) is satisfied.

$$\left(\left(V_1^* - V_o\right)K_{mu1} + E_N - V_o\right)\left(\alpha + \frac{\alpha}{sT_i}\right) + \beta I_o + \gamma I_C = I_1^* \quad (1)$$

Multiply the inner loop gain k and G_{PWM} together to from a new G_{PWM}. The inner current loop satisfies equation (2).

$$\left(\left(I_1^* - I_1\right)G_{PWM} - V_C\right)\frac{1}{sL_1} = I_1 \quad (2)$$

If G_{PWM} is much larger than 1, from equation (2), the reference current I_1^* is equal to I_1. Suppose $\gamma = G_{PWM}/\left(1+G_{PWM}\right)$. Then, equations 1-2 will be simplified and equation 3 is satisfied.

$$V_o = \frac{V_1^* K_{mu1} + E_N}{1+K_{mu1}} - \frac{1-\beta}{\alpha(1+K_{mu1})\left(1+\frac{1}{sT_i}\right)} I_o \quad (3)$$

From equation (3), the system is equivalent to Fig. 3. The output characteristic is equivalent to a voltage source with an inner output impedance. Equations (4)-(6) are expressions of the components in Fig. 3.

$$E_i = \frac{E_N + V_1^* K_{mu1}}{1+K_{mu1}} \quad (4)$$

$$R_i = \frac{1-\beta}{\alpha\left(1+K_{mu1}\right)} \quad (5)$$

$$L_i = R_i T_i \quad (6)$$

As shown in equations (4)-(6), all of the components of the equivalent circuit in Fig. 3 can be controlled accurately via setting certain control parameters.

From the analysis above, the V_1^* regulator keeps the system equivalent to a voltage source with an inner output impedance. The voltage source and the output impedance

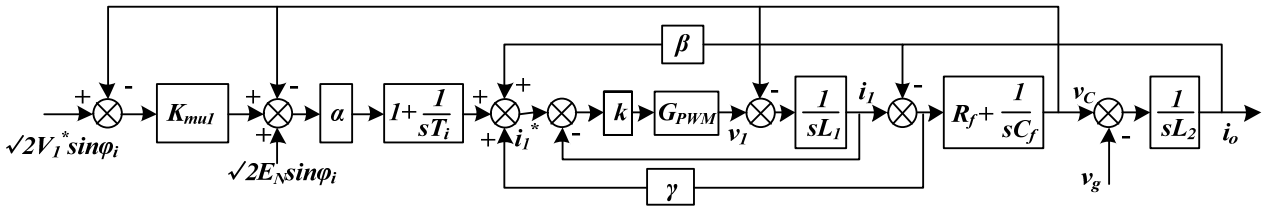

Fig. 2. Details of V_1^* regulator.

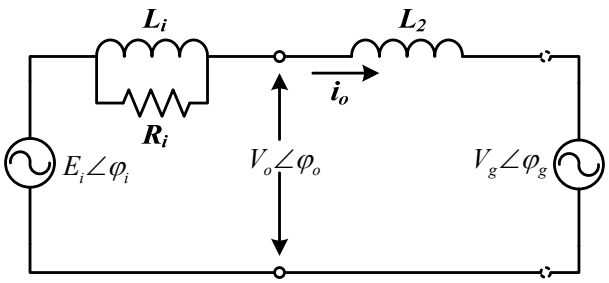

Fig. 3. Equivalent circuit of the system.

both can be controlled accurately by setting certain control parameters. Here in the distributed generations for microgrids, a small T_i will be chosen to make the output impedance inductive for output power decoupling. This will be further discussed in Section IV.

III. 2ND AXIAL VOLTAGE REGULATOR IN THE GRID-CONNECTED MODE

Details of the V_2^* regulator are shown in Fig 4. This regulator is responsible for the frequency regulation of the inverter. The phase information is sent to the voltage references in the V_1^* regulator. Here in this paper, the 1/4 period time delay quadrature signal generator is replaced by the second order generalized integrator (SOGI) method [14], [15]. Details of the SOGI are shown in Fig 5. It is a widely used quadrature signal generation method. It can help filter higher harmonic waves and has better performance when the grid frequency fluctuates. The dynamic response of the SOGI is faster as well.

The adoption of the SOGI improves the performance of the whole inverter. The improvement is shown in Fig 6. Parameters are chosen that are the same as those in Section V. The output power is P=800W and Q=600Var (at full load). Fig. 6(a), (c) are the inverter performances using the SOGI, while Fig. 6(b), (d) are the inverter performances using the 1/4 period time delay. Fig. 6(a), (b) show the situation of the frequency fluctuation. The grid frequency varies from 52Hz to 48Hz. The two figures show that the SOGI can output the grid frequency accurately, while the frequency of the 1/4 period time delay has a large 100Hz sinusoid fluctuation. Fig. 6(c), (d) show the performances with harmonic waves inside. 3th, 5th and 7th harmonic waves with the same amplitude of

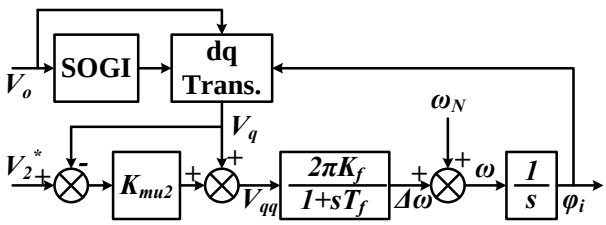

Fig. 4. Control block of V_2^* regulator.

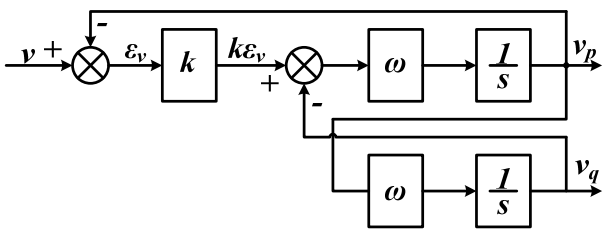

Fig. 5. Control block of SOGI.

11√2V are added into the grid voltage at t=2s. The THD of the voltage is up to 8.10%. The output frequency of the SOGI is accurate, and the output fluctuation is much smaller than that of the 1/4 period time delay.

Because of the adoption of the SOGI, the dynamic expressions of the output frequency and phase are changed in comparison with Reference 8. A small L_2 is chosen in Fig 1 so that $v_o \approx v_g$ is satisfied. Thus, $v_o(=V_o\sin\varphi_o)$ can be replaced by $v_g(=V_g\sin\varphi_g)$ from here on. Here in Fig. 4, Equation (7) is deduced by the SOGI and dq transformation.

$$v_q = V_g \sin\left(\varphi_g - \varphi_i\right) \approx V_g\left(\varphi_g - \varphi_i\right) \tag{7}$$

Given $\varphi_i-\varphi_g \approx 0$ and some simplification for Fig. 4, the following equation will be satisfied.

$$\omega_i(s) = \left(K_{mu2}\left(\frac{V_2^*}{s} - V_q(s)\right) + V_q(s)\right)\frac{2\pi K_f}{1+sT_f} + \frac{\omega_N}{s} \tag{8}$$

Simplify Equation (8) with Equation (7). Then, Equation (9) can be achieved.

$$\omega_i(s) = \frac{2\pi K_f\left(\left(1-K_{mu2}\right)V_g\omega_g + sK_{mu2}V_2^*\right) + s\left(1+sT_f\right)\omega_N}{s\left(s+s^2T_f+2\pi K_f\left(1-K_{mu2}\right)V_g\right)} \tag{9}$$

Thus, equation (10) is satisfied for steady state.

$$\lim_{t\to\infty}\omega_i(t) = \lim_{s\to 0} s\omega_i(s) = \omega_g \tag{10}$$

Hence, the inverter frequency will finally be the same as the grid if connected to the grid. The self-synchronous ability

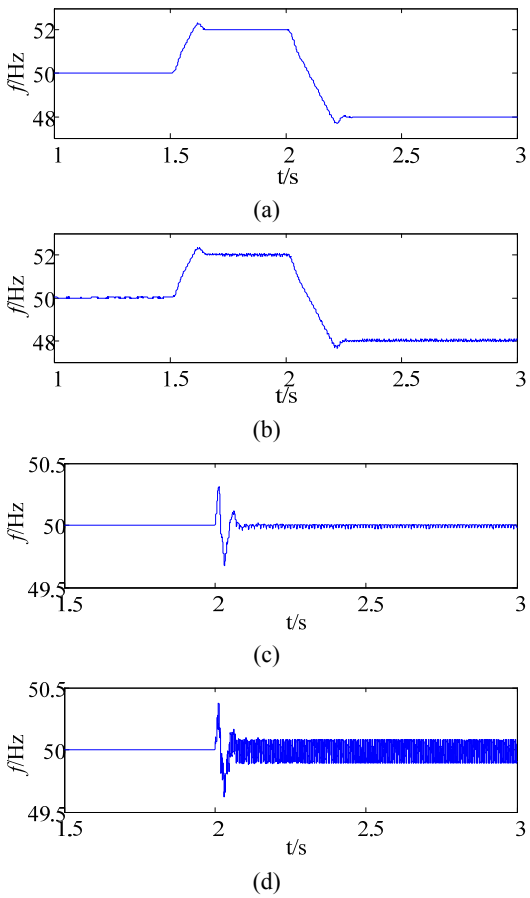

Fig. 6. Frequency response of SOGI and 1/4 period time delay.

remains.

Usually, the power angle δ determines the output power. The steady state value of δ is calculated as follows.

$$\lim_{t\to\infty}\delta(t)=\lim_{t\to\infty}(\varphi_i-\varphi_g)$$
$$=\frac{K_{mu2}}{(1-K_{mu2})V_g}V_2^*+\frac{\omega_N-\omega_g}{2\pi K_f(1-K_{mu2})V_g} \quad (11)$$

The expressions of the frequency and phase are greatly simplified when compared to reference (8). Given a certain V_2^* and no closed loop control, some conclusion can be made from equation 8 in the grid-connected mode.

1) If $\omega_N>\omega_g$, then δ has an escalating trend and active power tends to flow from the inverter to the grid. If $\omega_N<\omega_g$, the power trend is opposite.
2) If $V_2^*>0$, then δ has a rising trend and active power tends to flow from the inverter to the grid. If $V_2^*<0$, the trend is opposite.

IV. Axial Voltage Regulation for *PQ* Control

As mentioned in Section II, a small T_i is chosen to make the output impedance inductive. The line impedance and equivalent impedance of the grid is variable in microgrids. Different impedance characteristics have different output power characteristics. Thus a large enough α is necessary to offset the small transmission line impedance and the grid equivalent impedance. The resistive component of the whole impedance can be regarded as 0 by the choice of these control parameters. The expressions of the output power are as follows by Fig. 3.

$$P=\frac{E_iV_g\sin\delta}{X} \quad (12)$$

$$Q=\frac{E_iV_g\cos\delta-V_g^2}{X} \quad (13)$$

X is the total impedance between e_i and v_g in Fig. 3. It is mainly determined by the inner output impedance of the inverter. E_i and δ are the main control parameters that determine the output power. When in the grid connected mode, the output frequency ω_i will finally be the same as the grid frequency ω_g as shown in Section III. The steady state of the E_i and δ expressions are as follows.

$$\delta=\frac{K_{mu2}}{(1-K_{mu2})V_g}V_2^* \quad (14)$$

$$E_i=\frac{E_N+K_{mu1}V_1^*}{1+K_{mu1}} \quad (15)$$

E_i and δ are controlled separately by different axial voltage regulators. Partial derivatives for P & Q are figured out from equations (12) and (13) to evaluate the control impact of the regulators.

$$\partial P=\frac{E_iV_g\cos\delta}{X}\partial\delta+\frac{V_g\sin\delta}{X}\partial E_i$$
$$=\frac{V_g\sin\delta}{X}*\frac{K_{mu1}}{1+K_{mu1}}\partial V_1^*+\frac{E\cos\delta}{X}*\frac{K_{mu2}}{1-K_{mu2}}\partial V_2^* \quad (16)$$

$$\partial Q=\frac{V_g\cos\delta}{X}\partial E_i-\frac{E_iV_g\sin\delta}{X}\partial\delta$$
$$=\frac{V_g\cos\delta}{X}*\frac{K_{mu1}}{1+K_{mu1}}\partial V_1^*-\frac{E_i\sin\delta}{X}*\frac{K_{mu2}}{1-K_{mu2}}\partial V_2^* \quad (17)$$

Since δ is very small, *e*quations (16) and (17) show that V_1^* can control the output reactive power, while V_2^* controls the output active power. The relationship is linear. To evaluate the 2 axial voltage regulators' impact on power regulation more accurately, 3-dimensional *P/Q* VS. V_1^* & V_2^* figures are drawn. The main control parameters adopted are the same as those in Section V.

Fig. 6 and Fig. 7 show the relationship between the output *PQ* and V_1^* & V_2^*. Fig. 6 shows that the output active power is linearly controlled by V_2^*, and that V_1^* does not change *P*. Fig. 7 shows that the output reactive power is linearly controlled by V_1^*, ant that V_2^* does not change *Q*.

V. Simulation and Experimental Results

A simulation model based on the control strategy is built in

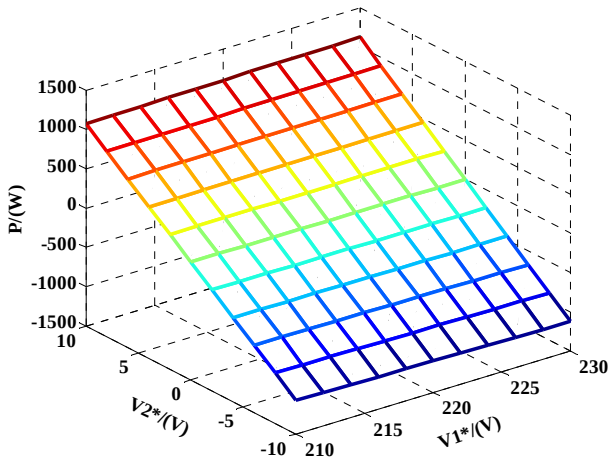

Fig. 7. Relationship between output P and V_1^*&V_2^*.

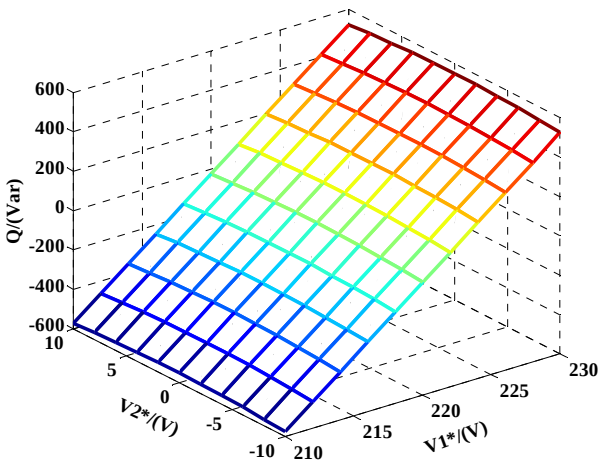

Fig. 8. Relationship between Output Q and V_1^*&V_2^*.

Matlab/Simulink. The simulation step size is 0.01ms. An Ode 45 is chosen as the solver, and the relative tolerance is 1e-4. The main simulation parameters are listed in Tables I and II. The rated power of the inverter is 1kVA. Just like the situation of a microgrid, the inverter is directly connected to the main grid with a breaker. No isolation transformer is adopted here.

By the parameters in Table I and II, the equivalent circuit impedance of Fig. 3 is a 10Ω resistor paralleled with a 2Ω inductor. The resistor is much larger than the inductor impedance. Thus, it can be neglected. The grid voltage RMS value is 220V, with a frequency of 50Hz. The circuit satisfies the following equation.

$$\dot{V}_o = \dot{E}_i - jX_i\dot{I}_o \tag{18}$$

Thus, the RMS values of the output voltage V_o and current I_o satisfy the following equation.

$$V_o^2 + X_i^2 I_o^2 = E_i^2 \tag{19}$$

To evaluate the output impedance of the inverter, different resistive loads (∞, 48Ω, 48/2Ω, 48/4Ω, 48/8Ω, 48/16Ω, 48/32Ω, 48/64Ω , and 0) are connected to the system. Fig. 8 shows the relationship between the RMS values of the output

TABLE I
PARAMETERS OF THE MAIN CIRCUIT

Parameters	Values
DC Source Voltage V_{DC}	400 V
Inverter-side Inductor L_1	5 mH
Grid-side Inductor L_2	0.2 mH
Capacitor C_f	47 μF
Damping Resistor R_f	0.5 Ω

TABLE II
MAIN CONTROL PARAMETERS

E_N/(V)	ω_N/(rad/s)	K_f	T_f/(s)	T_i/(ms)
220	50	0.01	0.001	0.636
α	β	γ	K_{mu1}	K_{mu2}
0.1	-1	1	1	0.5
k	k_{p1}	k_{i1}	k_{p2}	k_{i2}
20	0.001	0.5	0.01	0.1

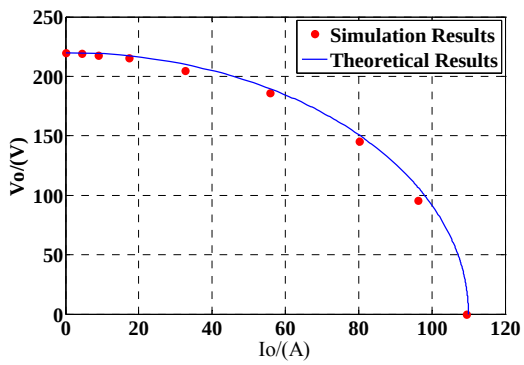

Fig. 9. Characteristics of output voltage and current.

voltage and current. The solid blue line is drawn from Equation (19). The simulation results satisfy theoretical analysis well.

To evaluate the control effects of V_1^* VS. Q and V_2^* VS. P, data with different PQs are measured and drawn in Fig. 10(a) and (b). The relationship between V_1^* VS. Q and V_2^* VS. P matches the theoretical analysis of Section IV from the figures.

Fig 11 shows the whole changing process of the power output and controller values. The PQ reference values all underwent step changes. The simulation starts at t=0. The system is synchronized and connected to the grid before t=1s. This process is not the paper's focus and is ignored. The P and Q references are all 0 in this process. The reference values change 4 times during the whole process. At t= 1.5s, P_{ref} is set as 500W, while Q_{ref} remains 0. At t= 2s, Q_{ref} jumps to 600Var, while P_{ref} remains 500W. At t= 2.5s, Q_{ref} steps to 800Var, and P_{ref} is still 500W. At t=3s, P_{ref} is set as 800W, while Q_{ref} remains 800Var. Fig. 11(a)-(f) shows the value changing process. Fig. 11(a)-(c) show the relationship of V_1^*-E_i-Q, while Fig. 11(d)-(f) show the relationship of V_2^*-f-P. The figures show that V_1^* controls E_i and Q, while V_2^* controls the frequency and P. The simulation results verify the theoretical analysis. Fig. 12 shows the decouple control of

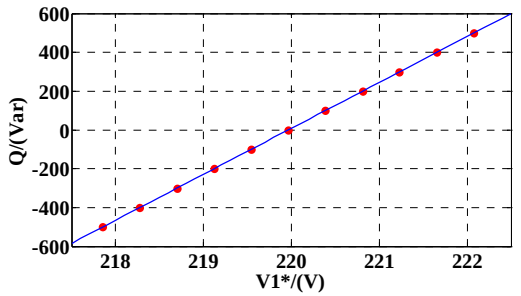

(a) V_1^* V.S. Q.

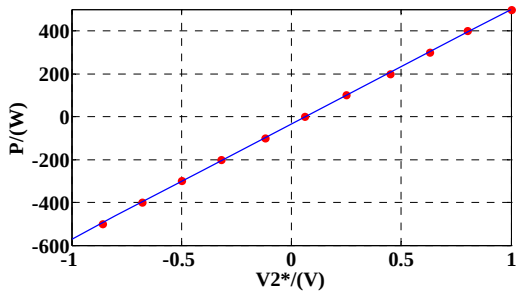

(b) V_2^* V.S. P.

Fig. 10. Simulation results of relationship between axial voltages and PQ output.

the PQ output. The PQ reference values change linearly and follow the ramp signals. The current is multiplied by 30 to match the amplitude of the voltage. The output P (Q) remains stable when the output Q (P) changes. The output voltage and current both transit very smoothly when the PQ references change. The PQ output decouples well.

To verify the idea, an experiment based on a TMS320F28335 is carried out. The main control parameters are the same as those applied in the simulation. The rated power of the inverter is also 1kVA. The inverter is connected to the grid via an isolation transformer. Fig. 13(a)-(c) are the different working status of the inverter. Fig. 13(a) shows the beginning of the work. The inverter is connected to the grid smoothly with a new seamless transfer strategy. This strategy will be the focus of another paper. The PQ references are both 0. The output voltage is almost the same as the grid voltage, and output current is fluctuating in a small scale around 0. The output P and Q are both close to 0. The inverter outputs active power only in Fig. 13(b). The output P is around 910W, and the fluctuation of output Q is 55Var. The current THD is around 4%. Power coefficient is 0.998. The inverter outputs reactive power only in Fig. 13(c). The output P fluctuation is 30W, and the output Q is around 880Var. The THD of the output current rises a little to around 5%. This still satisfies the general standard. The terminal voltage rises to around 220V (nominal value), and is much higher than that in Fig. 13(b). The power quality is remarkably improved. The inverter outputs almost the same power as the reference values. The transient process when P_{ref} is changing is shown in Fig. 13(d). Output current and voltage remain high quality.

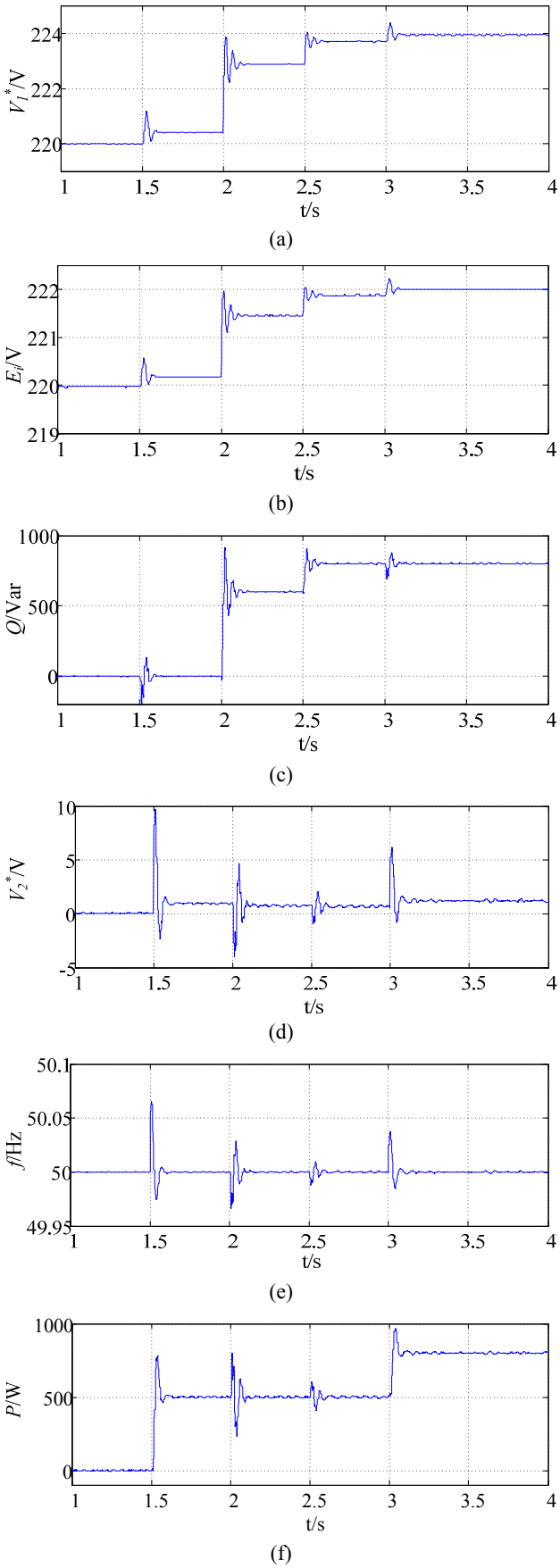

Fig. 11. System response with step reference change.

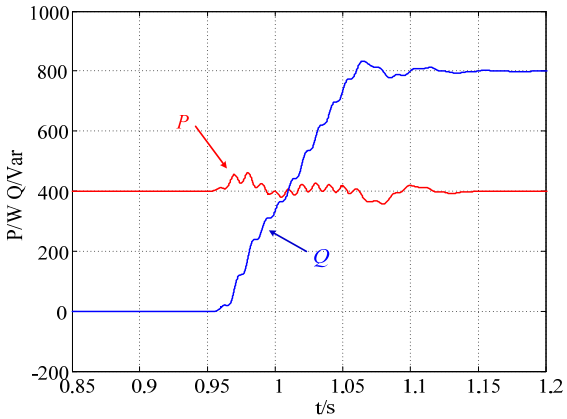

(a)

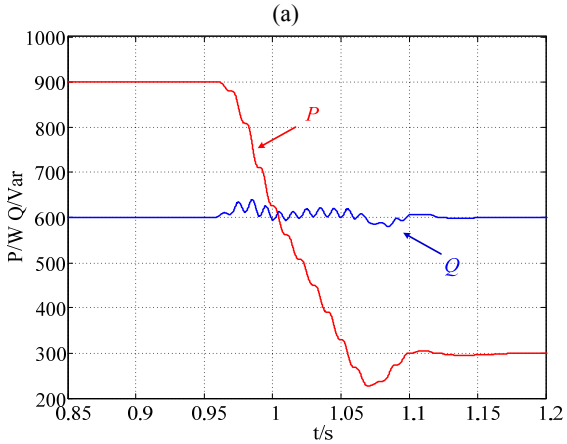

(b)

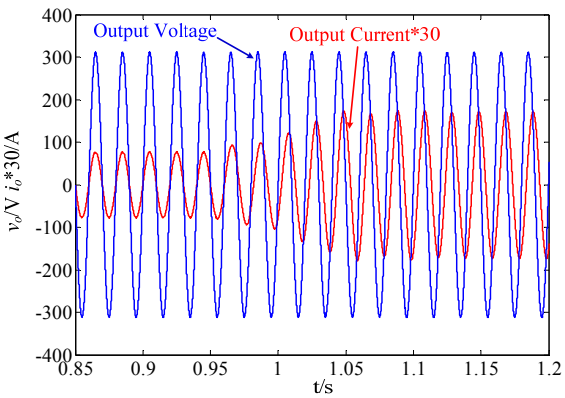

(c)

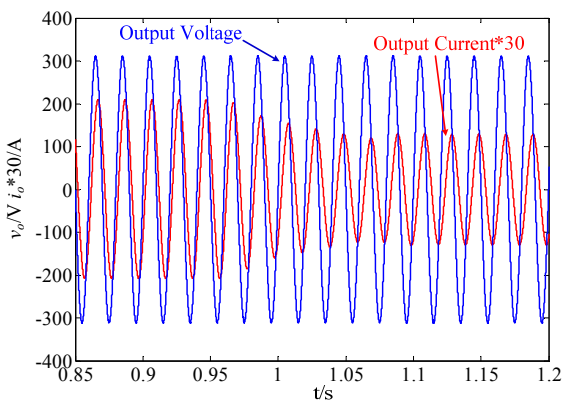

(d)

Fig. 12. Decoupling Effect of PQ Output.

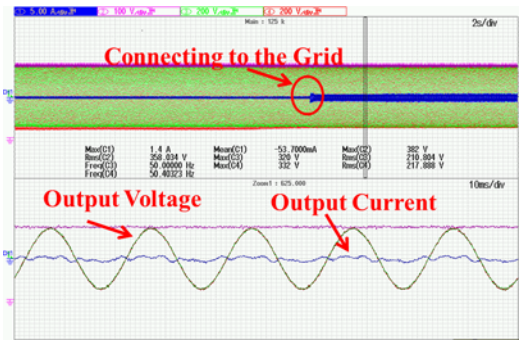

(a) P_{ref} = 0, Q_{ref} = 0.

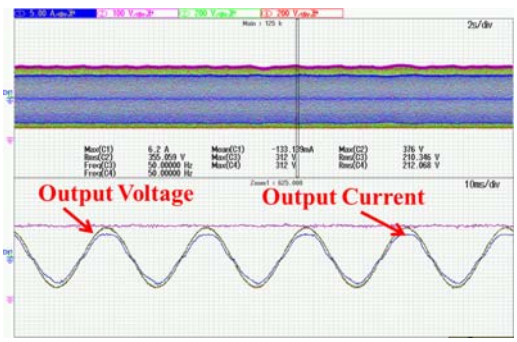

(b) P_{ref} =900W, Q_{ref} = 0.

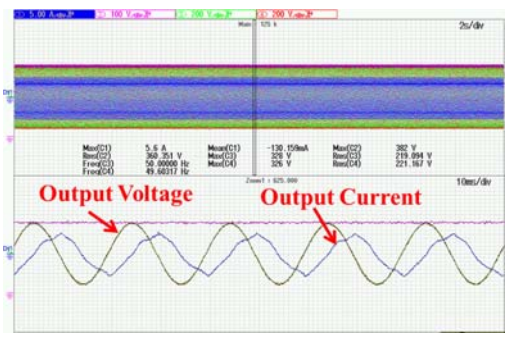

(c) P_{ref}=0, Q_{ref} =900Var.

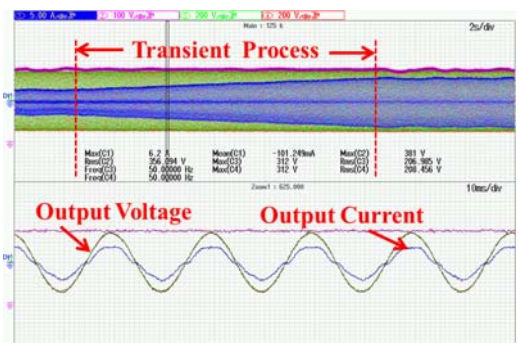

(d) Transition Process of P_{ref} from 500W to 900W.

Fig. 13. *PQ* output of the experiment.

VI. CONCLUSION

A PQ control strategy for a microgrid inverter with axial voltage regulators is raised in the paper. The inverter is voltage controlled and has 2 axial voltage regulators. The 1st regulator controls the output voltage and the 2nd controls the output frequency. The output *P* is controlled by the 2nd axial

voltage regulator, and the output Q is controlled by the 1st axial voltage regulator. P and Q are decoupled well with proper control parameters. The control strategy is discussed in detail and verified by simulation and experimental results. The inverter has good characteristics for application in microgrid development.

ACKNOWLEDGMENT

The authors would like to thank for the financial support of the Shanghai Talent Development Fund (*Grant No. 2012024*), the Innovation Program of Shanghai Municipal Education Commission (*Grant No. 13ZZ132*) and Shanghai Engineering Research Center of Green Energy Grid-Connected Technology *(Grant No. 13DZ2251900)*.

REFERENCES

[1] N. Hatziargyriou, "Microgrids." *IEEE Power and Energy Mag.,* Vol. 5, No. 4, pp. 78-94, Apr. 2007.
[2] X. Q. Li, X. J. Wu, Y. W. Geng, Q. Zhang, "Stability analysis of grid-connected inverters with an LCL filter considering grid impedance," *Journal of Power Electronics*, Vol. 13, No. 5, pp. 896-908, Oct. 2013.
[3] C. Bao, X. Ruan, X. Wang, D. Pan, W. Li, and K. Weng, "Design of grid-connected inverters with LCL filter based on PI regulator and capacitor current feedback active damping." in *Proc. of the CSEE*. Vol. 32. No. 25, 2012.
[4] Y. Wu, J. Kan, and S. Xie, "Control strategy for grid-connected inverter based on double d-q coordinates," *Transactions of CES,* Vol. 26, No. 8, pp. 106-112, Aug. 2011.
[5] R. Yan, and K. S. Tapan. "Investigation of voltage stability for residential customers due to high photovoltaic penetrations," *IEEE Trans. Power Syst.,* Vol. 27, No. 2, pp. 651-662, Feb. 2012.
[6] H. Kim, T. Yu, and S. Choi, "Indirect current control algorithm for utility interactive inverters in distributed generation systems," *IEEE Trans. Power Electron.,* Vol. 23, No. 3, pp. 1342-1347, Mar. 2008.
[7] Y. Wu, J. Kan, and S. Xie, "An indirect current control scheme for grid-connected inverter with regulation of active power to phase and reactive power to voltage amplitude," *Automation of Electric Power Systems,* Vol. 35 No. 11, pp. 93-97, Nov. 2011.
[8] J. H. Im, S. H. Song, and S. Kang. "Analysis and compensation of PCC voltage variations caused by wind turbine power fluctuations," *Journal of Power Electronics*, Vol. 13, No. 5, pp. 854-860, Oct. 2013.
[9] Y. W. Li and C. N. Kao. "An accurate power control strategy for power-electronics-interfaced distributed generation units operating in a low-voltage multibus microgrid," *IEEE Trans. Power Electronics,* Vol. 24, No.12, pp. 2977-2988, Dec. 2009.
[10] F. Gao and M. R. Iravani. "A control strategy for a distributed generation unit in grid-connected and autonomous modes of operation," *IEEE Trans. Power Del.,* Vol. 23, No. 2, pp. 850-859, Feb. 2008.
[11] Q. C. Zhong, and G. Weiss, "Synchronverters: Inverters that mimic synchronous generators," *IEEE Trans. Ind. Electron.,* Vol. 58, No. 4 pp. 1259-1267, Apr. 2011.
[12] J. Hu, J. Zhu, D. G. Dorrell, et al. "Virtual flux droop method – A new control strategy of inverters in microgrids," *IEEE Trans. Power Electron.,* Vol. 29, No. 9, pp. 4704-4711, Sep. 2014.
[13] J. B. Zhao, S. Ushiki, and M. Ohshima, "Grid-connected inverter with inner output impedance and governor-free characteristics," in *Proc. Energy Conversion Congress and Exposition*, 2010.
[14] J. S. Park, T. H. Nguyen, and D. C. Lee. "Advanced SOGI-FLL scheme based on fuzzy logic for single-phase grid-connected converters," *Journal of Power Electronics*, Vol. 14, No. 3, pp. 598-607, May 2014.
[15] I. Carugati, P. Donato, S. Maestri, D. Carrica, and M. Benedetti, "Frequency adaptive PLL for polluted single-phase grids," *IEEE Trans. Power Electron.,* Vol. 27, No. 5 pp. 2396-2404, May 2012.

Yang Chen was born in China, in 1990. He received his B.S. degree in Electrical Engineering from Zhejiang University, Zhejiang, China, in 2012. He is presently working towards his M.S. degree at the Shanghai University of Electric Power, Shanghai, China. He worked as an Engineer for the Nari-Relays Corporation, Nanjing, China, from 2012 to 2013. His current research interests include the modeling and control of inverters, and distributed power generation in microgrids.

Jinbin Zhao (M'06) was born in China, in 1972. He received his M.S. and Ph.D. degrees in Electrical Engineering from Oita University, Oita, Japan, in 2002 and 2005, respectively. He worked as a Researcher at the R&D Headquarters of Origin Electric Co., Ltd, Japan, from 2005 to 2011. He is presently working as a Professor at the Shanghai University of Electric Power, Shanghai, China. His current research interests include the control of power converters, soft-switching power converters, inverters, distributed power systems, power-factor correction, and electric drive systems. Dr. Zhao is a Member of the IEEJ and IEICE of Japan as well as a Senior Member of the CPSS.

Keqing Qu was born in China, in 1970. He received his Ph.D. degree in Electrical Engineering from Shanghai University, Shanghai, China, in 2004. He is presently working as an Associate Professor at the Shanghai University of Electric Power, Shanghai, China. He is also a Master Instructor. He studied in Germany as a Visiting Scholar with full funding by the national foundation, from 2009 to 2010. His current research interests include power electronic conversion, and new energy generation and its application to power systems.

Fen Li received her B.S. and Ph.D. degrees in Electrical Engineering from the Huazhong University of Science and Technology, Wuhan, China, in 2005 and 2010, respectively. She has been an Engineer in the Hubei Meteorological Bureau, Wuhan, China, since 2010. She is presently working as a Lecturer at the Shanghai University of Electric Power, Shanghai, China. Her current research interests include high power factor converters, the grid-connected control of renewable energy power generation, solar resource evaluation and forecast, the relationship between photovoltaic power and meteorological factors, and PV power prediction.